THE JOURNAL OF PHYSICAL CHEMISTRY B

Article

pubs.acs.org/JPCB

Enhanced Sensitivity by Nonuniform Sampling Enables Multidimensional MAS NMR Spectroscopy of Protein Assemblies

Sivakumar Paramasivam,[†,∥] Christopher L. Suiter,[†,‡,∥] Guangjin Hou,[†,‡] Shangjin Sun,[†,§] Melissa Palmer,[⊥] Jeffrey C. Hoch,[¶] David Rovnyak,*[,⊥] and Tatyana Polenova*[,†,‡]

[†]Department of Chemistry and Biochemistry, University of Delaware, Newark, Delaware 19716, United States

[‡]Pittsburgh Center for HIV Protein Interactions, University of Pittsburgh School of Medicine, Pittsburgh, Pennsylvania 15261, United States

[⊥]Department of Chemistry, Bucknell University, Lewisburg, Pennsylvania 17837, United States

[¶]Department of Molecular, Microbial, and Structural Biology, University of Connecticut Health Center, 263 Farmington Avenue, Farmington, Connecticut 06030-3305, United States

Supporting Information

ABSTRACT: We report dramatic sensitivity enhancements in multidimensional MAS NMR spectra by the use of nonuniform sampling (NUS) and introduce maximum entropy interpolation (MINT) processing that assures the linearity between the time and frequency domains of the NUS acquired data sets. A systematic analysis of sensitivity and resolution in 2D and 3D NUS spectra reveals that with NUS, at least 1.5- to 2-fold sensitivity enhancement can be attained in each indirect dimension without compromising the spectral resolution. These enhancements are similar to or higher than those attained by the newest-generation commercial cryogenic probes. We explore the benefits of this NUS/MaxEnt approach in proteins and protein assemblies using 1−73-(U-^{13}C,^{15}N)/74−108-(U-^{15}N) *Escherichia coli* thioredoxin reassembly. We demonstrate that in thioredoxin reassembly, NUS permits acquisition of high-quality 3D-NCACX spectra, which are inaccessible with conventional sampling due to prohibitively long experiment times. Of critical importance, issues that hinder NUS-based SNR enhancement in 3D-NMR of liquids are mitigated in the study of solid samples in which theoretical enhancements on the order of 3−4 fold are accessible by compounding the NUS-based SNR enhancement of each indirect dimension. NUS/MINT is anticipated to be widely applicable and advantageous for multidimensional heteronuclear MAS NMR spectroscopy of proteins, protein assemblies, and other biological systems.

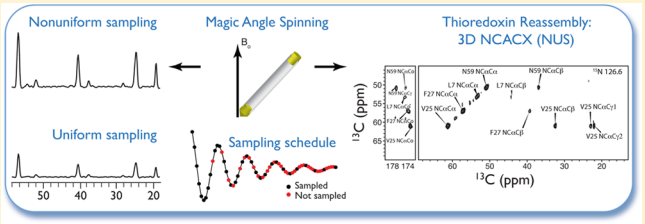

INTRODUCTION

Multidimensional correlation spectroscopy is at the core of NMR-based structure and dynamics studies in biomacromolecules, be it in solution or in the solid state. In solid-state protein NMR, acquisition of a full set of multidimensional spectra for structure determination requires weeks and is often impractical in low-sensitivity systems. The long experiment times are in part due to the requirement for equidistant sampling of time-domain indirect-dimension points on a Nyquist grid for fast Fourier transform (FFT) to generate frequency-domain spectra.

Nonconventional nonuniform sampling (NUS) methods have been employed in NMR and MRI previously.[1−6] In NUS, the time-domain signal need not be sampled on a uniform Cartesian grid, and the experiment time is considerably shortened by reducing the sampling density. These samples can be acquired either according to off-grid or on-grid schedules (e.g., random vs radial), and time-domain signals acquired with such nonuniform schedules require alternative spectral processing algorithms other than discrete Fourier transform. The choice of a processing algorithm depends on whether the data were acquired off-grid or on-grid, and the currently available reconstruction methods include maximum entropy (MaxEnt),[7−17] maximum likelihood (ML),[18] forward maximum entropy reconstruction (FM),[19,20] covariance transform,[21] projection reconstruction,[3] G-matrix Fourier transform,[6] spectroscopy by integration of frequency and time domain information,[22] multidimensional decomposition,[23] filter diagonalization,[24] and others. In addition to time savings due to the grid sparseness, NUS gives rise to true time- and frequency-domain sensitivity enhancements, the extent of which can be controlled by the design of sampling schedules relative to the decay time constant of the FID (determined by either T_2 or T_2^*, depending on the particular experiment).[25,26]

NUS/MaxEnt protocols are well established in solution, yet this approach is not widely applied in multidimensional solid-state NMR spectroscopy.[27−33] Solid-state NMR of biomacromolecules faces additional challenges of lower sensitivity and decreased resolution due to residual homonuclear and heteronuclear dipolar interactions broadening the spectral lines

Received: April 5, 2012
Revised: June 1, 2012
Published: June 5, 2012

or due to conformational heterogeneity present in interesting biological samples.[34−52] Recent reports indicate that NUS can yield solid-state NMR spectra of similar or higher quality than the conventional, linear sampling protocols.[28,29,31,32] Importantly, for the reasons discussed in this work, multidimensional solid-state NMR is uniquely suited to take the best advantage from NUS, and there is a need for systematic analysis of sensitivity and resolution in SSNMR NUS spectra.

Here, we report large sensitivity gains attained by nonuniform sampling in multidimensional (2D and 3D) magic angle spinning (MAS) NMR spectroscopy. We introduce the concept of maximum entropy interpolation (MINT), in which entropy maximization is used to estimate the values of missing data samples, while tightly constraining the resulting spectrum to closely match the measured samples in random, exponentially biased NUS schemes. In a model tripeptide MLF and in 1−73-(U-^{13}C,^{15}N)/74−108-(U-^{15}N) *Escherichia coli* thioredoxin reassembly, we demonstrate that for the same total experiment time, NUS yields a 1.5−2.0-fold sensitivity increase in each indirect dimension, and the net gain depends upon the sampling schedule, in accord with previous reports.[26] These sensitivity enhancements are similar to or higher than those attained by the newest generation commercial cryogenic probes. With carefully designed NUS schedules, sensitivity gains are obtained without compromising spectral resolution. In thioredoxin reassembly, NUS permits acquisition of excellent-quality 3D spectra, which is impossible with uniform sampling because of prohibitively long experiment times.

Our results demonstrate the promise of the NUS/MINT approach for significantly enhancing sensitivity and enabling multidimensional SSNMR spectroscopy of challenging biological systems, such as protein assemblies and membrane proteins.

EXPERIMENTS AND METHODS

Materials. All chemicals were purchased from Sigma Aldrich. U-$^{13}C_6$ -glucose and $^{15}NH_4Cl$, as well as the tripeptide MLF were purchased from Cambridge Isotope Laboratories (Andover, MA, US), and used without any further recrystallization. The media used for *E. coli* cultures was purchased from Oxoid, Inc. (Nepean, ON, CA). Each reagent was used without further purification.

MLF and Thioredoxin Reassembly Sample Preparation. Approximately 9 mg (20.6 μmol) of the MLF powder was packed into a 3.2 mm Varian MAS rotor and sealed with an upper spacer and a top spinner.

Preparation of a solid-state NMR sample of 1−73-(U-^{13}C,^{15}N)/74−108-(U-^{15}N) reassembled thioredoxin by controlled precipitation was reported previously.[53−58] First, two batches of *E. coli* cells containing thioredoxin expression system were grown in M9 minimal media: (i) U-^{13}C,^{15}N isotopically labeled, and (ii) U-^{15}N isotopically labeled. Thioredoxin was purified from both batches according to the previously reported protocols,[59] and the final yields of the purified protein were 40 and 100 mg/L of minimal media for the U-^{13}C,^{15}N-enriched, and U-^{15}N-enriched thioredoxin, respectively.[56] The pure thioredoxin from each batch was subsequently proteolytically cleaved at the Arg-73 site as reported previously.[59] Next, the complementary fragments consisting of the N-terminal residues 1−73 and the C-terminal residues 74−108 were purified. Each U-^{13}C,^{15}N-enriched fragment was then reconstituted with its complementary U-^{15}N-enriched counterpart, resulting in two reassembled thioredoxin samples: 1−73-(U-^{13}C,^{15}N)/74−108(U-^{15}N) and 1−73(U-^{15}N)/74−108-(U-^{13}C,^{15}N). A controlled precipitation protocol[54] was followed to generate the hydrated nanocrystalline sample of 1−73-(U-^{13}C,^{15}N)/74−108-(U-^{15}N) reassembled thioredoxin. Eleven milligrams of this reassembled thioredoxin sample was packed into a 3.2 mm Varian MAS rotor and sealed with an upper spacer and a top spinner.

NMR Spectroscopy. All solid-state NMR spectra were acquired on a 14.1 T narrow bore Varian InfinityPlus spectrometer operating at Larmor frequencies of 599.8 (^{1}H), 150.8 (^{13}C), and 60.8 (^{15}N) MHz. All experiments were performed using a 3.2 mm Varian triple-resonance T3 probe. The MAS frequency for each experiment was set to 10 kHz and controlled to ±2 Hz by a Varian MAS controller. The temperature was set to +20 and −5 °C for MLF and thioredoxin samples, respectively, and was controlled to ±0.1 °C by a Varian temperature controller. ^{13}C and ^{15}N chemical shifts were referenced with respect to external standards adamantane and ammonium chloride, respectively. Typical pulse lengths were 2.5 μs for ^{1}H, and 3.3 μs for ^{13}C. ^{1}H−X (X = ^{13}C or ^{15}N) cross-polarization was achieved by applying a linearly ramped radio frequency (rf) field on the X nucleus and a constant-amplitude rf field on ^{1}H. For heteronuclear NCA and NCACX experiments, SPECIFIC−CP with a tangent amplitude ramp was used to selectively transfer magnetization from ^{15}N to $^{13}C^{\alpha}$. CP and SPECIFIC−CP conditions were optimized to attain the first-order Hartmann−Hahn matching condition. The ^{1}H−^{15}N and ^{15}N−^{13}C contact times were 1.5 and 6.2 ms, respectively. TPPM decoupling was used in all cases, with a rf field strength of 90 kHz. In 2D and 3D NCACX experiments, a DARR mixing time of 15 ms was used for C^{α}−CX transfer. Recycle delays were set at 3 s for all experiments. In all cases, States detection[60] was employed for phase-sensitive detection in the indirect dimensions.

Two-dimensional uniformly sampled (US) spectra of MLF were collected as (1000 × 64) complex matrices with 4 and 24 transients per t_1 increment for NCA and NCACX data sets, respectively. Two-dimensional NUS NCA and NCACX spectra of MLF were collected as (1000 × 32) complex matrices with 8 and 48 transients per t_1 increment for NCA and NCACX data, respectively. In the case of US data, each of the 64 t_1 increments was sampled along an equally spaced interval of 480 μs until the final acquisition time of 30.2 ms. For NUS spectra, the 32 t_1 increments (50% of US data points) were distributed in either random or biased-random fashion with the final sampled data point also set at 30.2 ms. We will refer to the distributions of points in the NUS-collected data for the 2D heteronuclear experiments as NUS1 and NUS2, schematically shown in Figure S1 of the Supporting Information. In the NUS1 schedule, the first 8 of 32 points are forced to be uniform; the remaining 24 points are distributed nonuniformly up to 30.2 ms. The sampled points in NUS1 are taken at time intervals of (0, 1, 2, 3, 4, 5, 6, 7, 8, 10, 11, 12, 14, 15, 17, 19, 20, 22, 24, 26, 28, 30, 32, 35, 37, 40, 43, 46, 50, 54, 58, 63) × dw (dw = 480 μs). In the NUS2 schedule, all 32 points except for the first point are distributed nonuniformly for the same total evolution time (30.2 ms). The sampled points in NUS2 are taken at time intervals of: (0, 2, 4, 5, 6, 7, 8, 10, 11, 15, 16, 22, 23, 25, 27, 28, 29, 30, 32, 36, 38, 40, 41, 43, 49, 50, 54, 55, 57, 59, 60, 63) × dw (dw = 480 μs). Since we measured the ^{15}N T_2* of MLF to be about 10 ms, the total evolution time of 30.2 ms matches the $3T_2^*$ limit required for maximal resolution.[26] By setting the acquisition times equal and doubling the number of transients in the NUS data, the total experimental time between a pair of data sets was equivalent permitting a direct comparison of the spectra.

dx.doi.org/10.1021/jp3032786 | J. Phys. Chem. B 2012, 116, 7416−7427

Three-dimensional uniformly sampled NCACX spectra of MLF were collected as (1000 × 36 × 36) complex matrices with 8 transients per t_1 or t_2 increment. Three-dimensional NUS NCACX spectra of MLF were collected as (1000 × 324) hypercomplex matrices with the 324 indirect dimensions points constructed according to a random exponentially biased schedule with 32 transients per t_1 or t_2 increment. For uniformly sampled 3D NCACX experiments, the maximum evolution time in both indirect dimensions was 8.75 ms. For NUS 3D NCACX experiments, the points were distributed in an exponentially biased random fashion (see below) with the final sampled data point corresponding to 8.75 ms in both indirect dimensions. In total, 324 of the 1296 possible points (25% of US data points) were recorded. A schematic representation of the 3D NUS schedule is presented in the Supporting Information (Figure S1).

Two-dimensional NCA data for 1−73-(U-^{13}C,^{15}N)/74−108-(U-^{15}N) reassembled thioredoxin were collected as (1000 × 64) and (1000 × 32) complex matrices for US and NUS experiments, respectively. The final data point in each case was sampled at an acquisition time of 30.2 ms; 32 and 64 transients per t_1 increment were collected for US and NUS protocols, respectively. NUS1 was used for data collection of 2D NCA spectra. Two-dimensional NCACX spectra for 1−73-(U-^{13}C,^{15}N)/74−108-(U-^{15}N) reassembled thioredoxin were collected as (1000 × 128) and (1000 × 64) complex matrices following US and NUS protocols, respectively, with the final data point acquired at 20.3 ms; 256 and 512 transients per t_1 increment were recorded for US and NUS protocols, respectively. For the NUS 2D NCACX experiment, a random exponentially biased schedule containing 64 out of 128 points was used, which we will refer to as NUS3.

Three-dimensional NCACX spectra for 1−73-(U-^{13}C,^{15}N)/74−108-(U-^{15}N) reassembled thioredoxin were collected as a (1000 x 324) hypercomplex matrix with the 324 indirect dimensions points constructed according to a random exponentially biased schedule with 128 transients per t_1 or t_2 increment, and the final data points were acquired at 11.2 ms for ^{15}N, and 5.6 ms for ^{13}C. We did not collect a uniformly sampled data set for this experiment because of the prohibitively long time required to attain appropriate sensitivity. The NUS schedule used for this data set collection is the same as described for the three-dimensional NCA and NCACX experiments on MLF (shown in Figure S1 of the Supporting Information).

The NUS schedules used in the experiments were created using the ScheduleTool program developed by Mark Maciejewski and colleagues (http://sbtools.uchc.edu/nmr/sample_scheduler/). The NUS1, NUS2, and NUS3 schedules used for the collection of 2D data on MLF and 1−73-(U-^{13}C,^{15}N)/74−108-(U-^{15}N) reassembled thioredoxin were exponentially weighted in the indirect dimension by assuming a 45 Hz decay rate. The NUS schedule used for the collection of 3D data (dubbed NUS3D) was exponentially weighted in both indirect dimensions, using decay rates of 45 Hz. The sample schedules were then integrated into the pulse sequences used for data collection and Rowland NMR Toolkit (RNMRTK, software documentation available at http://rnmrtk.uchc.edu)[61] scripts used for processing.

NMR Data Processing and Analysis. All spectra were processed using the RNMRTK software package and then analyzed using SPARKY3.[62]

Generally, for data sampled uniformly in the indirect dimensions, FFT was used to process both the direct and the indirect dimensions using RNMRTK. For data sets in which nonuniform sampling was employed in the indirect dimensions, as mentioned above, FFT processing is not applicable. In these cases, we processed the direct dimension using FFT and the indirect dimensions using either MINT or MaxEnt reconstruction with the processing script reflecting the appropriate sampling schedule.

For two-dimensional spectra collected on MLF, 60° sinebell-squared shifted apodizations followed by Lorentzian-to-Gaussian transformations were applied in the direct dimension for all spectra. In the direct dimensions, zero-filling to 2048 points was used in all cases. For 2D MLF spectra, data were processed without any zero-filling for intensity comparisons (to perform FFT/MINT transformation with the same number of points as in the experiment). However, for the comparison of resolution of NUS/MINT spectra against US/FFT method, zero-filling up to 128 points was employed to increase the digital resolution of the spectra. In the case of NUS/MINT, in addition to appending 64 zeros in the time-domain data in the indirect dimension, their positions (65−128) were also included in the NUS schedule files NUS1 and NUS2. For three-dimensional NCACX spectra of MLF, a cosine window function followed by Lorentzian-to-Gaussian apodization was applied in the direct dimension. Data were zero-filled up to 2048 points in the direct dimension. In the $t_1 \times t_2$ dimensions of the NCACX experiment, zero-filling up to 64 × 64 points was applied for both FFT and MaxEnt spectra. Zero filling the indirect dimensions of the 3D NUS data was done in conjunction with including the position of zeros (37−64) in the schedule file for both indirect dimensions.

For two-dimensional NCA and NCACX data collected on 1−73-(U-^{13}C,^{15}N)/74−108-(U-^{15}N) reassembled thioredoxin, 45° sinebell-squared shifted apodizations followed by Lorentzian-to-Gaussian transformations were applied in the direct dimensions. The data were zero-filled to 2048 and 512 points in the direct and indirect dimensions, respectively. For three-dimensional NCACX data, 60° sinebell-squared shifted apodization was applied in the direct dimension, and zero-filling to 128 points was used in the indirect dimensions.

BACKGROUND AND THEORY

The basic NMR signal is an exponentially decaying sinusoid. The frequency of oscillation denotes only the chemical shift, so the exponential decay of the signal in the time domain prescribes the magnitude of the signal. The SNR for a uniformly sampled free induction decay (FID) has been derived and experimentally confirmed previously for uniform sampling to vary with time according to[25]

$$\mathrm{SNR} \propto \frac{T_2(1 - e^{-t_{max}/T_2})}{\sqrt{t_{max}}} \quad (1)$$

where T_2 (or in solids, T_2^*) is the transverse decay constant and t_{max} is the duration of acquisition, and the solution is presented in the limit of continuous sampling. Solving for the maximum yields the ideal SNR at about $1.26T_2$.

In uniform sampling, the sampling density is a constant and may be arbitrarily set as unity for the duration of the FID. In nonuniform sampling, the sampling density is allowed to vary. For this work, we employ sampling densities decaying monoexponentially, although other sampling densities may be worth further investigation. To compare the results from uniform and NUS *n*D-NMR experiments, the total experimental time must be equal. Considering the indirect dimension of a two-dimensional NMR experiment, the total time depends on the degree of evolution in the indirect dimensions and upon the

number of scans per t_1 increment. We introduce and solve for a scaling factor χ, such that the areas under the uniform and NUS sampling density curves are equal,[26]

$$\chi = \frac{\alpha(T_2/T_{SMP})}{1 - e^{-\alpha T_2/T_{SMP}}} \quad (2)$$

where T_{SMP} is the exponential decay constant for the sampling density, and the evolution is parametrized by T_2 via $\alpha = t_{max}/T_2$. In other words, taking $S(t) = e^{-t/T_2}$ as our uniformly sampled FID, since it is scaled by unity, the NUS-scaled FID, which consumes the identical experimental time, is given by $\chi\, S(t)$.

Taking the ratio of the uniform and nonuniform signal areas, we obtain the enhancement of the SNR in the time domain,[26]

$$\eta = \frac{\chi(1 - e^{-\alpha((T_2/T_{SMP})+1)})}{(T_2/T_{SMP} + 1)(1 - e^{-\alpha})} \quad (3)$$

For matched NUS, where $T_{SMP} = T_2$ and for optimal signal resolution ($t_{max} = \pi T_2$), the predicted enhancement in the time domain data is a factor of 1.7. For a T_{SMP}/T_2 ratio of 2 and $t_{max} = \pi T_2$, the predicted enhancement is 2.2 (see Figure 1A). Further biasing NUS beyond $T_{SMP} > 2T_2$ generally does not offer compelling improvements in the SNR enhancement of the FID.

The enhancement of eq 3 for exponentially weighted NUS can be generalized for the use of any nonuniform sampling density $h(t)$, which is assumed to be continuous and bounded over t_{max}, such as in Gaussian densities.[63] To enforce equal total acquisition times for uniform and nonuniform sampling, we define a constant χ as satisfying

$$t_{max} = \chi \int_0^{t_{max}} h(t)\, dt \quad (4)$$

which ensures that the areas under the graphs of $f(t) = t_{max}$ and $g(t) = \chi\, h(t)$ are equivalent,[26] requiring then

$$\chi = \frac{t_{max}}{\int_0^{t_{max}} h(t)\, dt} \quad (5)$$

where χ has the effect of ensuring that equal numbers of transients are considered in the uniform and nonuniform cases so that the total noise is equivalent in these two cases. Then the theoretical SNR enhancement for any NUS density $h(t)$ applied to an exponentially decaying signal over an evolution period spanned by t_{max} is obtained by only taking the ratio of the integrated signal intensities,

$$\eta = \frac{\int_0^{t_{max}} \chi\, h(t)\, e^{-t/T_2}\, dt}{\int_0^{t_{max}} e^{-t/T_2}\, dt} = \frac{\chi \int_0^{t_{max}} h(t)\, e^{-t/T_2}\, dt}{T_2(1 - e^{-t_{max}/T_2})} \quad (6)$$

Small variations in the experimentally realized enhancement occur since the discretized sampling scheme cannot perfectly match the ideal continuous sampling density $h(t)$.[26]

For any realized sampling scheme corresponding to a subset of samples from the uniform sampling set given by a sampling function $\mathbf{k}$ having the value 1 for sampled times and zero for times not sampled, the sensitivity $R(\mathbf{k})$ of the sampling scheme relative to uniform sampling is given by

$$R(\mathbf{k}) = \frac{\sum_{i=1}^{N} k_i p_i}{\sum_{i=1}^{N} p_i} \quad (7)$$

where the elements of $\mathbf{p}$ are given by

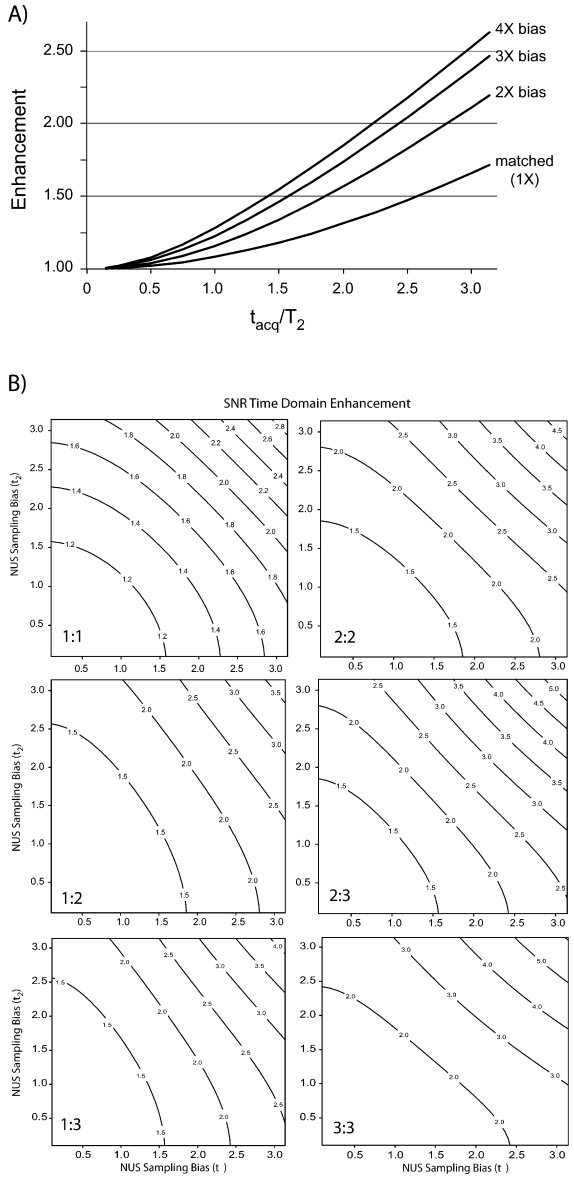

Figure 1. (A) The theoretical SNR enhancement in the time domain of one dimension as a function of t_{max} for matched, 2-, 3-, and 4-fold sampling biases. As the T_{SMP}/T_2 ratio increases, predicted enhancement grows as a result of the acquisition of more signal at times that are short compared with T_2. However, once the NUS bias reaches up to $3T_2$ and $4T_2$, further improvement on enhancement is negligible. The ability to obtain the theoretical enhancement is also constrained by how closely the discretized NUS sampling schedule conforms to the prescribed exponential NUS sampling density.[26] (B) In this series of six 3D contour graphs, the x-axis is the evolution period α for the second dimension, the y-axis represents α for the third dimension, and the z-axis (shown via the contour lines) represents the compounded SNR enhancement of the time domain data for NUS in both indirect dimensions. The bias of the exponential nonuniform sampling relative to the signal decay in each dimension is indicated in each panel. So 1:1 is matched exponential NUS in each dimension, and 1:3 would be matched in t_1 and 3-fold biased in t_2. If both dimensions were allowed to acquire until $t_{max} = \pi T_2$, the predicted compounded enhancement could reach 3−5 fold.

$$p_i = \exp\left\{i\left(\frac{i - 1}{T_2 \times SW}\right)\right\} \quad (8)$$

dx.doi.org/10.1021/jp3032786 | J. Phys. Chem. B 2012, 116, 7416−7427

with spectral width SW. Equations 7 and 8 readily generalize to multiple dimensions.[1]

It is evident then that for 3D NMR, both the second and third dimensions could be enhanced by NUS, provided that each dimension exhibits a decaying signal. A compounded enhancement would then be obtained as

$$\eta = \eta(\alpha_2, (T_2/T_{SMP})_2) \times \eta(\alpha_1, (T_2/T_{SMP})_1) \quad (9)$$

where α_2 and α_1 are the maximum evolution periods in the respective indirect dimensions. The compounded enhancements predicted by eq 9 and for a variety of exponential NUS schemes are presented in Figure 1B. Under optimal conditions, the predicted enhancements over two indirect dimensions are on the order of 3−5 -fold.

However, solution state *n*D-NMR will fall far short of fully exploiting eq 9. Specifically, both indirect dimensions must be sampled to about $3T_2$ to obtain such high improvements, yet in liquids, it is often prohibitive to reach even T_2 in both indirect dimensions of 3D-NMR.[25] Further, it should be evident from the preceding discussion that the origin of the SNR enhancement by NUS is the exploitation of the signal decay so that no enhancement can be obtained in any constant-time dimensions,[26] which are a staple of multidimensional solution state NMR. At present, there is little potential to obtain compounded SNR enhancements by performing NUS in 3D-NMR experiments in liquids. However, a much different situation exists for solid phase samples. For example, for solid samples at or near room temperature, the heteronuclear T_2 values are often on the order of tens of milliseconds so that it is feasible for α to approach $\sim 3T_2$ for both indirect dimensions within plausible total experimental times. Further, constant-time periods are not commonly employed in biosolids pulse sequences so that both indirect dimensions are available for NUS-based SNR enhancement. That is, in biosolids 3D-NMR, we have the potential to access enhancements of the time domain predicted by eq 9 up to 3−5-fold with NUS, comparable to those obtained with cryogenic probes in liquid samples. This is demonstrated in the current work.

RESULTS AND DISCUSSION

Sensitivity: General Considerations. Direct comparison of peak intensities in the spectra processed with MaxEnt vs FFT is not generally valid because of the inherent nonlinearity of the MaxEnt reconstruction. Frequency-domain intensity is generally a nonlinear function of time-domain intensity, with the relationships between the two signals being dependent upon the MaxEnt parameters (internally specified as *def* and λ in RNMRTK).[61] These parameters are uniquely optimized for every data set, and a direct estimate of intensity enhancement of NUS/MaxEnt data with respect to US/FFT data is not as straightforward as measuring SNR.

However, the generally nonlinear spectral response of the MaxEnt can be rendered nearly linear by reconstructing the MaxEnt spectra with λ set to an arbitrarily high, constant value. λ is a Lagrange multiplier of the constraint that the difference between the inverse Fourier transform of the MaxEnt spectra and the experimental FID be minimal. By increasing λ, more weight is given to the constraint function of the inverse Fourier transform (the experimental data) than to maximizing the entropy functional, and in the limit of very high λ values, MaxEnt spectra approach the FFT spectra and become identical for uniform sampling. This is illustrated in Figure S2 of the Supporting Information, depicting f1 projections of the 2D NCA spectra of MLF processed with FFT and MaxEnt (λ = 50). The FFT and MaxEnt spectra are indistinguishable within the numerical precision of the data sets.

The same processing strategy is extended to the nonuniformly sampled data acquired with NUS1, NUS2, and NUS3 sampling schedules, for which 50% of the data points are collected in the indirect dimension of the 2D experiments. Spectral reconstruction of the NUS data with a large value of the λ parameter is expected to give rise to the same linear behavior as discussed above, and hence, spectral intensities of the NUS MaxEnt spectra can be directly compared with the uniformly sampled FFT spectra to get an estimate of intensity enhancement obtained in the NUS protocol over the same experiment time, as discussed below.

In the limit of large λ, the result of MaxEnt reconstruction for uniformly sampled data approaches the zero-filled FFT. In this regime, the mock data (the inverse FFT of the MaxEnt spectrum) are constrained to tightly match the measured data. This amounts to overfitting because an independent measurement of the data will contain a different realization of the noise, with the consequence that the mock data for the first MaxEnt spectrum will not agree with the second set of measured data. Although no statistical significance can be attached to features in the MaxEnt spectrum in the large-λ limit, the result is highly linear, and statistical tests for significance can be applied post hoc.

Now consider MaxEnt reconstruction in the large-λ limit for NUS data. Here, the mock data are constrained to tightly match the measured data, and the elements of the mock data corresponding to unmeasured data values are determined exclusively by maximizing the entropy. By analogy to maximum entropy extrapolation,[64] we refer to MaxEnt reconstruction in the large-λ limit as maximum entropy interpolation (MINT). It is important to note that high-λ "MaxEnt" in principle violates the basic tenet of MaxEnt reconstruction, which is that the MaxEnt spectrum is the one containing the least amount of information that is consistent with the experimental data.[11] Consistency means "agrees with to within the experimental uncertainty", not "matches exactly". Thus, features in MaxEnt spectra are statistically significant.

At high λ, the resulting spectrum is overfit to the data, in the sense that repeating the experiment will produce a data set that is not consistent with the high-λ MaxEnt spectrum of the first experiment. It is thus important to clearly distinguish high-λ MaxEnt and MaxEnt the statistical method. Ni and Scheraga used the maximum entropy principle to determine how to extrapolate a uniformly sampled signal to longer times; the result was the first demonstration of linear prediction (LP) extrapolation.[64] Since LP extrapolation leaves the measured data untouched, as does high-λ MaxEnt, the term "maximum entropy interpolation" (MINT) used to describe high-λ MaxEnt applied to NUS data is apt, and it (the acronym MINT) serves to distinguish high-λ MaxEnt from the statistical method known as MaxEnt reconstruction. Although LP extrapolation enjoyed considerable success as a method for reducing truncation artifacts in multidimensional spectra, it is well-known to be prone to generating false peaks for noisy data and for yielding biased frequencies when the signals are not perfectly Lorentzian (strict exponential decay). MaxEnt has been shown to be more robust than LP, according to several criteria.[65]

We note that MINT is similar to forward maximum entropy (FM) described by Hyberts and Wagner,[20] with several important distinctions. The entropy functional we employ[16] is convex and everywhere differentiable, in contrast to that

dx.doi.org/10.1021/jp3032786 | J. Phys. Chem. B 2012, 116, 7416−7427

Table 1. Noise Reduction and Intensity Enhancement in Nonuniformly Sampled 2D Heteronuclear Correlation Spectra of MLF

spectrum	method	noise rmsd	relative noise[a]	residue	correlation	intensity enhancement[b]
2D NCA	FFT	188	1.00			
	MINT (NUS1)	128	(1/1.47)	M	$N-C^{\alpha}$	2.14
				L	$N-C^{\alpha}$	2.06
				F	$N-C^{\alpha}$	2.01
	MINT (NUS2)	131	(1/1.44)	M	$N-C^{\alpha}$	1.82
				L	$N-C^{\alpha}$	1.82
				F	$N-C^{\alpha}$	1.81
2D NCACX	FFT	464	1.00			
	MINT (NUS1)	324	(1/1.43)	M	$N-C^{\alpha}/N-C^{\beta}/N-C^{\gamma}/N-C^{O}$	2.11/2.16/1.93/2.23
				L	$N-C^{\alpha}/N-C^{\beta}/N-C^{\gamma}/N-C^{\delta}/N-C^{O}$	1.97/2.02/1.98/1.92/1.95
				F	$N-C^{\alpha}/N-C^{\beta}/N-C^{O}$	1.93/2.03/2.06
	MINT (NUS2)	324	(1/1.43)	M	$N-C^{\alpha}/N-C^{\beta}/N-C^{\gamma}/N-C^{O}$	1.71/1.58/1.52/1.74
				L	$N-C^{\alpha}/N-C^{\beta}/N-C^{\gamma}/N-C^{\delta}/N-C^{O}$	1.77/1.72/1.63/1.54/1.60
				F	$N-C^{\alpha}/N-C^{\beta}/N-C^{O}$	1.62/1.80/1.53

[a]Relative noise is defined as the ratio of the actual noise in a particular data set (either US/FFT or NUS/MINT) to the actual noise in the corresponding US/FFT data set. In all cases, noise was measured with 8064 samples of a blank region of the 2D spectra. The NUS spectra were generated from the uniformly sampled data set by extracting 50% points in the indirect dimension according to sampling schedules NUS1/NUS2 and processing it with MaxEnt reconstruction using $\lambda = 50$. [b]Intensity enhancement is calculated as the intensity ratio in the nonuniformly vs uniformly sampled data set acquired with the same total experiment time.

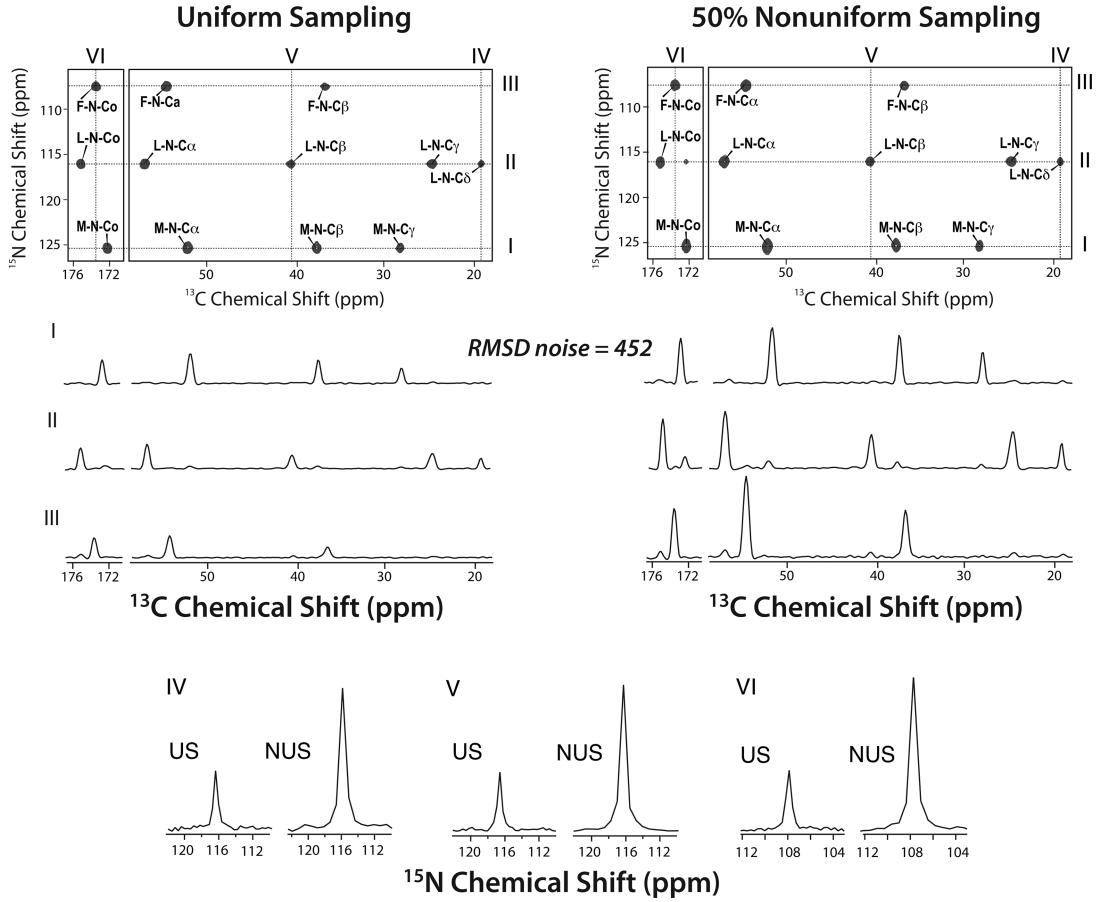

Figure 2. Comparison of 2D NCACX spectra of MLF: top left, sampled uniformly (as a 1000 × 64 complex matrix, 4 transients per increment), and top right, nonuniformly in the indirect dimension (as a 1000 × 32 complex matrix, 8 transients per increment, using NUS1 sampling schedule). The rms noise levels in the 2D NUS and US spectra are the same. Roman numerals I, II, and III correspond to 1D slices extracted along the direct dimensions for residues M, L, and F, respectively. Roman numerals IV, V, and VI correspond to 1D slices extracted along the indirect dimension for $L-C^{\delta}$, $L-C^{\beta}$, and $F-C^{O}$, respectively. It can be seen that in each case, the NUS data set yields an increase in peak intensity when compared to the uniformly sampled slices displayed at the same noise level.

employed by the original implementation of FM, which is not differentiable at zero. Another difference is that we utilize existing MaxEnt code based on the Cambridge algorithm to compute MINT.[8,61] The algorithm employs analytic gradients and Hessians to achieve computational efficiency orders of magnitude greater than the FM approach of using numerical

dx.doi.org/10.1021/jp3032786 | J. Phys. Chem. B 2012, 116, 7416−7427

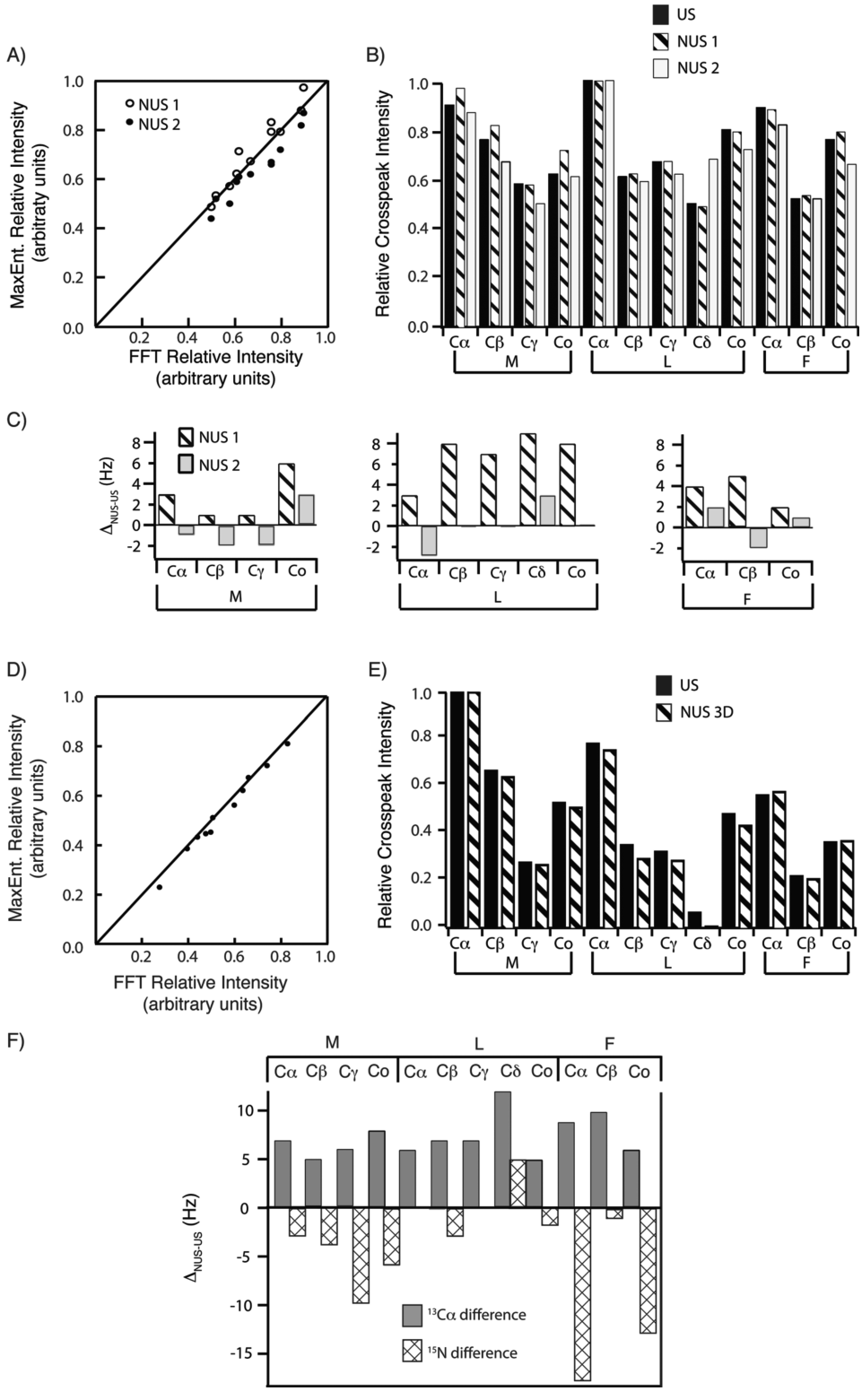

Figure 3. (A) Correlation plot of the relative cross-peak intensities of 2D NCACX spectra collected/processed with US/FFT and NUS/MINT (sampling schedules NUS1 and NUS2). (B) The same data presented as a bar graph. Black bars represent relative intensities in the FFT spectrum. Crossed bars and white bars represent the relative peak intensities in the NUS spectra for the two schedules NUS1 and NUS2, respectively. λ was set equal to 50 for MaxEnt processing of NUS1 and NUS2 spectra. (C) The differences in the ^{15}N line widths (f1 dimension) between MaxEnt spectra (acquired with schedules NUS1 and NUS2) and the FFT spectrum are shown for the three residues of MLF. (D) Correlation plot of relative cross-peak intensities of 3D NCACX spectra collected/processed with US/FFT and NUS/MINT methods. Since the 3D US NCACX data set was collected for the MLF sample as a 36 × 36 complex matrix in the two indirect dimensions ($t_1 \times t_2$), the corresponding frequency domain spectrum generated with FFT is at a minimum a 64 × 64 matrix due to the necessary zero-filling. To generate identical 3D MaxEnt spectra for the same US data set, we appended zeros in the data file from points 37 to 64 in each of the t_1 and t_2 dimensions and performed MINT reconstruction in t_1 and t_2 dimensions with λ of 5000. The resulting 3D MINT spectrum is identical to the 3D FFT spectrum of the same 3D US time-domain data. This is illustrated in Figure S3 of the Supporting

dx.doi.org/10.1021/jp3032786 | J. Phys. Chem. B 2012, 116, 7416−7427

Figure 3. continued

Information for three cross-peaks of the Leucine residue of MLF. The NUS schedule for 3D NCACX retained 25% (324) of the total number of points in the $t_1 \times t_2$ dimensions acquired in the corresponding US data set above. (E) The same data are presented as a bar graph. Black bars represent relative intensities in the US/FFT spectrum, and crossed bars represent the relative peak intensities in the NUS/MINT spectra. (F) The differences in the ^{13}C (f1 dimension) and ^{15}N (f2 dimension) line widths between NUS/MINT and US/FFT spectra are shown for the three residues of MLF. Note the opposite trend in the ^{15}N and ^{13}C line width differences in comparison to FFT spectra, which can possibly be due to two reasons. First, the nonuniform sampling schedule in the $t_1 \times t_2$ dimensions may not have been completely optimized for maximal resolution in both indirect dimensions. Second and perhaps more important is the different T_2^* relaxation times of the ^{15}N and $^{13}C^{\alpha}$ coherences. The maximum evolution time is 8.75 ms (250 μs × 35) in both indirect dimensions. Although this value might satisfy the $3T_2^*$ criterion for the ^{13}C dimension with the ^{13}C T_2^* being only a few milliseconds, it is not sufficiently long for the ^{15}N dimension with the ^{15}N T_2^* being ~10 ms. Hence, it is important to sample up to the $3T_2^*$ limit in each of the indirect dimensions in a multidimensional NUS experiment to attain maximal resolution in the NUS spectra.

derivatives. We note that the recent implementation of FM also uses analytic gradients. Convergence of MINT is tested on the basis of the values of the gradients, rather than the iterative step size, to detect premature convergence in which the step size becomes small before the objective function reaches the optimum. Convexity of the entropy functional ensures the existence of a unique solution.

Sensitivity: Noise Reduction. The signal-to-noise ratio (SNR) of an exponentially decaying FID with a decay constant T_2^* is a function of acquisition length of the FID. SNR reaches its maximum value at $t_{max} \sim 1.26T_2^*$ (discussed above and in ref 26). The total noise is directly proportional to the square root of the length of the FID or of the number of data points in the FID for a given acquisition length.

For the same number of transients, the total noise scales down as the square root of the ratio between the number of points in the NUS and US data set. For the NUS1 and NUS2 schedules (50% sampling) used in our 2D NCA and NCACX experiments, total noise reduction by a factor of $\sqrt{2}$ in the time domain is expected. To attain the same reduction in the frequency domain of the NUS spectra, the MaxEnt transformation should have the same linearity as FFT. MINT processing meets this criterion, and as illustrated in Table 1, the experimental results in MLF indeed yield the expected $\sqrt{2}$ noise reduction.

Sensitivity: Intensity Enhancement. As discussed above, the noise reduction in the NUS data sets contributes significantly to the increase in SNR of NUS spectra. Another factor determining the effective sensitivity in the NUS data sets is the total signal intensity, which also depends on the sampling schedule.

Intensity enhancement in NUS can be conveniently assessed by analysis of US/FFT and NUS/MINT experiments performed over the same experiment time. Reduction in the number of samples is compensated by increased number of transients in the NUS experiment, and increased intensity corresponds directly to increased SNR. Table 1 illustrates that the intensity enhancement in 2D NUS spectra collected over the same experiment time as US data sets is a function of the sampling schedule, in agreement with previous reports.[65] As discussed above and previously,[26] for exponentially decaying sampling density profiles, the intensity enhancement is 1.7 when the decay constant of the sampling density function matches the T_2^* of the FID and the total evolution time is $3T_2^*$. The enhancement can be higher than 2.0 when the above decay constant is twice or more the T_2^* of the FID. For the 2D spectra of MLF (Table 1 and Figure 2), the intensity enhancement is close to 2.0 or higher for the NUS1 schedule, indicating that the effective decay constant for this schedule is twice the ^{15}N T_2^*. For NUS2, the increase in intensity is 1.5−1.8, depending on the cross-peak type.

The net enhancement from NUS in 3D experiments can be as high as 3−5 fold over the corresponding US data sets acquired over the same time (see Background and ref 26). The actual enhancement is critically dependent upon the sampling schedule and the maximum evolution times in the two indirect dimensions relative to the respective T_2 values of the coherences. For 3D NCACX spectra of MLF (for NUS3D schedule, see Figure S1 of the Supporting Information), we observed enhancement factors of 2.7−3.3 for the MINT-processed spectra (λ = 5000 was selected for the same linearity as US/FFT, see Figure S3 of the Supporting Information).

We also note that when data sets possess high dynamic range or when signal intensities are comparable to the noise level, the probability of detection of weak peaks (which is related to sensitivity) can be assessed by repeating the same experiment multiple times, as described by Hyberts et al.[66]

Sensitivity: Relative Cross-Peak Intensities in NUS Spectra. The SNR of the time and frequency domain data are nonequivalent when nonlinear processing methods such as MaxEnt are used.[17,61] However, the relative peak intensities defined with respect to some large peak in the same spectrum are a valid measure of nonlinearity of the MaxEnt method. In Figure 3, 2D NCACX cross-peak intensities for MLF are plotted relative to that of Leu(N−C^{α}), the strongest resonance in the spectrum. The relative cross-peak intensities in the NUS1/MaxEnt (λ = 50) data are either the same as or slightly (by up to 13%) higher than the corresponding values in the FFT spectra. For NUS2/MaxEnt data, the relative intensities are generally weaker, by up to 14%. These differences in relative intensities, while not negligible, are in the acceptable range, at least for correlation spectra in which peak position is more important than peak intensity (e.g., those used for resonance assignments or for establishing qualitative distance constraints).

The comparison of relative cross-peak intensities in the 3D US/FFT and NUS/MINT NCACX spectra of MLF is shown in Figure 3D−E. The deviations of the relative peak heights between the two sets of spectra are typically in the range of 1−10%, with only one outlier whose relative intensity differs by as much as 17% between the two data sets. The intensity differences between the two 3D data sets are somewhat greater than the maximum deviations observed in the 2D NCACX spectra for schedules NUS1 (13%) and NUS2 (14%). Notably, the largest deviation (17%) is observed for the leucine (C^{δ}) peak, which has the lowest intensity in the 3D NCACX spectrum. Overall, the relative cross-peak intensities in the NUS data set are lower by 5% on average compared with those in the FFT spectrum.

Spectral Resolution. Resolution in the NUS spectra processed with MaxEnt reconstruction is also strongly dependent on the sampling schedule. There remains a trade-off between sensitivity and resolution, and in designing a sampling schedule,

dx.doi.org/10.1021/jp3032786 | J. Phys. Chem. B 2012, 116, 7416−7427

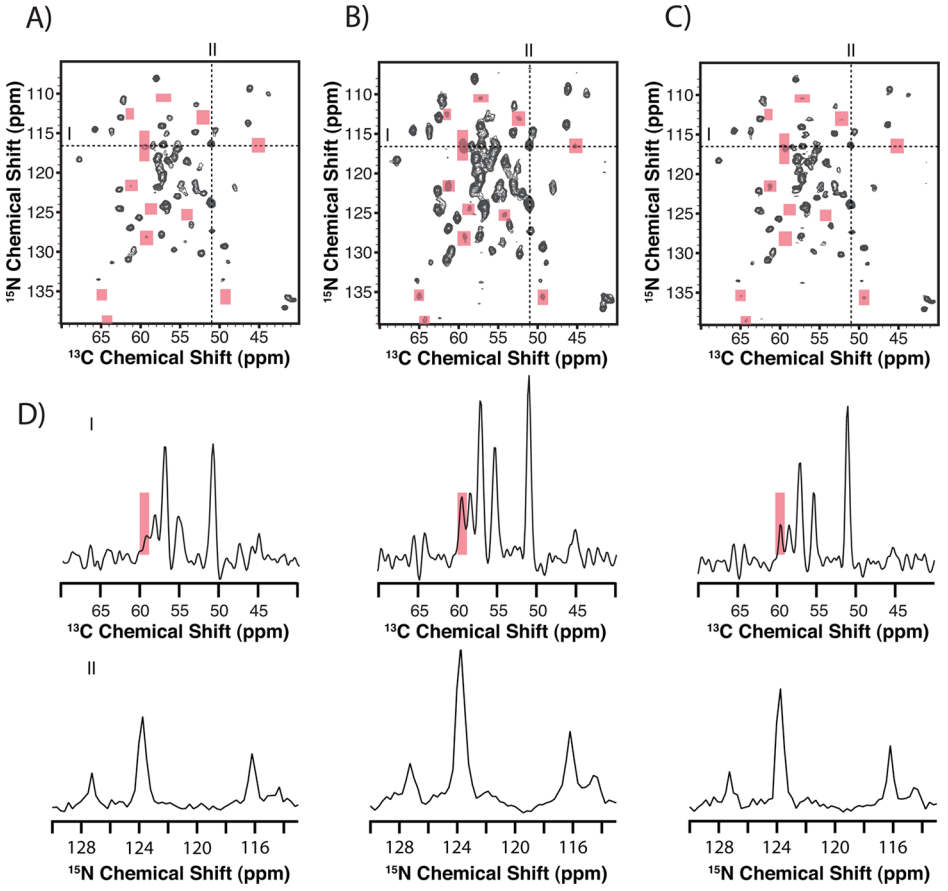

Figure 4. Comparison of 2D NCA spectra of 1−73-(U-^{13}C,^{15}N)/74−108-(U-^{15}N) thioredoxin reassembly: (A) collected with uniform sampling and processed with MINT, (B) collected with NUS1 sampling schedule and processed with MINT, and (C) collected with NUS1 sampling schedule and processed with MINT with 15 Hz line width deconvolution. Lineshapes extracted from the direct and indirect dimensions are labeled with Roman numerals I and II, respectively. The noise rms levels are equivalent in the US and NUS spectra processed without the line width deconvolution. The first contour in all spectra is set at 5 times the noise level in all data sets, and the level multiplier is 1.4. A significant increase in sensitivity is observed for both NUS data sets. The resolution is recovered by applying line width deconvolution in the indirect dimension. New peaks in NUS spectra are indicated with pink boxes.

one aims at either maximizing sensitivity or retaining the same resolution as in the FFT spectra while some sensitivity enhancement is attained. In our work, the NUS1 schedule was optimized for maximum sensitivity by equidistantly spacing the first 8 out of the total 32 points. The remaining 24 points are distributed randomly and nonuniformly. The NUS2 schedule was designed so that the frequency-domain spectra retain the same resolution as the US/FFT spectra, with all 32 points, but the first distributed randomly and nonuniformly.

As shown in Figure 3C, the ^{15}N line widths in the 2D NCACX spectra of MLF acquired with schedule NUS1 are consistently greater (by 1−9 and 5 Hz on average) than those in the corresponding US/FFT spectra. The corresponding spectrum acquired with schedule NUS2 retains the same resolution as FFT spectra, with a maximum deviation of only 3 Hz, which is negligible. Interestingly, the maximum deviation for both schedules (9 Hz for NUS1 and 3 Hz for NUS2) is observed for the weakest correlation in the 2D NCACX spectra (Leu-C$^{\delta}$).

The comparison of cross-peak line widths in the 3D US/FFT and NUS/MINT NCACX spectra is shown in Figure 3F. The line widths of the NUS/MINT spectra in the ^{15}N dimension are greater by 5−12 Hz than in the US/FFT spectra. In contrast, the line widths in the ^{13}C dimension are slightly smaller compared with US/FFT spectra for almost all cross-peaks except Leu C$^{\delta}$, the weakest correlation in the 3D NCACX spectra. Since the actual ^{13}C$^{\alpha}$ line widths for the 12 cross-peaks are, on average, ∼120 Hz, the observed line width improvement over the FFT spectra is only a few percent, and for all practical purposes, the resolution of the NUS C$^{\alpha}$ dimension can be considered the same as in FFT spectra.

It is important to design a nonuniform sampling schedule on a needs-dependent basis. The 2D schedules employed in this work followed two different goals. In the NUS1 schedule, a bias toward data collection at short evolution times in the indirect dimension(s) maximizes the sensitivity by increasing peak intensity at the expense of spectral resolution. In contrast, the NUS2 schedule demonstrates that collecting more points at long evolution times in the indirect dimension(s) retains the same spectral resolution while signal intensities and, hence, the overall sensitivity are somewhat reduced. It is important to be judicious when choosing how many points to retain in the NUS schedule compared with the equidistant Cartesian grid. As suggested previously,[33] as many as 50−75% of uniformly sampled points could be eliminated for NUS acquisition in every dimension, with the number of points retained depending on the dwell time in the indirect dimensions and the inherent sensitivity of a particular experiment. For this work, we followed a conservative approach by retaining 50% of the data points in each of the indirect dimensions.

dx.doi.org/10.1021/jp3032786 | J. Phys. Chem. B 2012, 116, 7416−7427

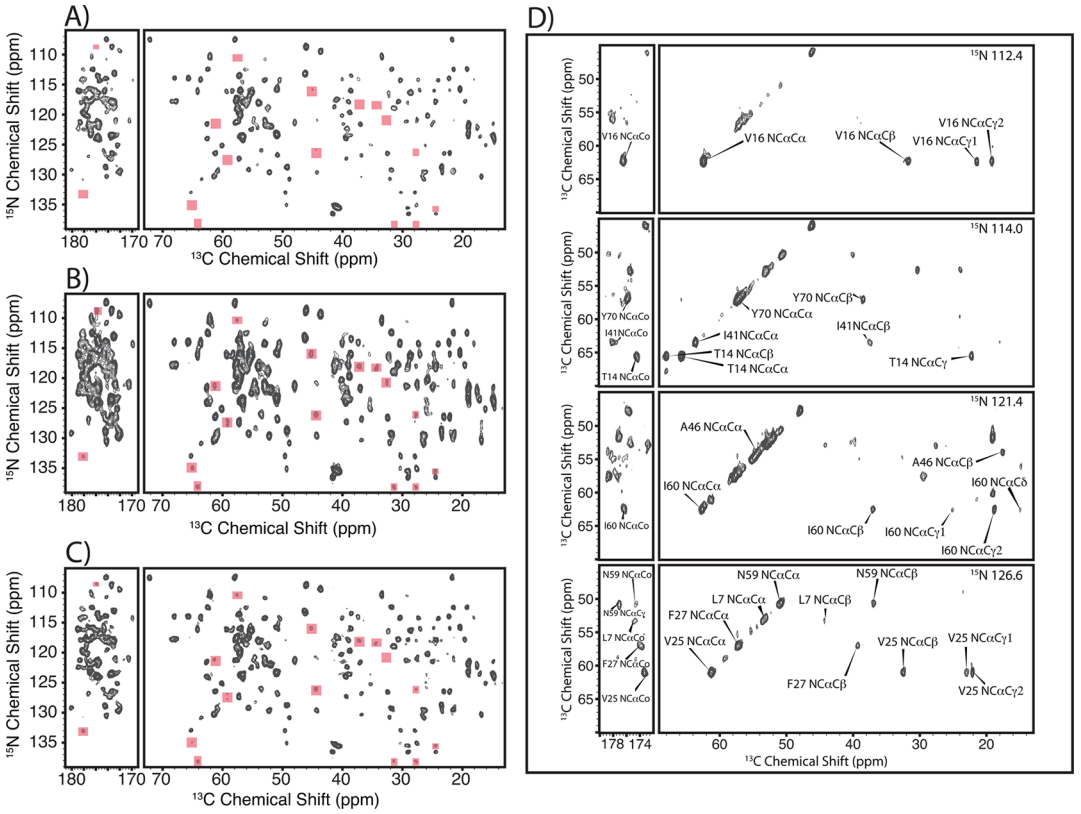

Figure 5. 2D and 3D NCACX spectra of 1−73-(U-^{13}C,^{15}N)/74−108-(U-^{15}N) thioredoxin reassembly. (A) 2D NCACX spectrum acquired by uniform sampling as a (1000 × 128) complex matrix using 256 transients per increment. 45° shifted sinebell squared apodization followed by Gaussian-to-Lorentzian transformation was utilized in the direct dimension, with zero-filling to 2048 points. Zero-filling to 512 points was used in the indirect dimension. The final data point was collected at 20.3 ms. (B) 2D NCACX spectrum acquired with 512 transients per increment as a (1000 × 64) complex matrix by nonuniform sampling using NUS3 schedule and processed with MINT using λ = 300. The final data point was collected at 20.3 ms. The same apodization and zero-filling parameters were used as in spectrum A. New peaks in NUS spectra are indicated with pink boxes. (C) This spectrum was collected and processed in the same manner as in B, except for the 25 Hz line width deconvolution applied in the indirect dimension, which improves the spectral resolution at the expense of losing some of the weaker signals. (D) Slices containing resonance assignments for a 3D NCACX (for full list of assignments see ref 56) experiment acquired as a (1000 × 324) hypercomplex matrix with the 324 indirect dimensions points constructed according to a random exponentially biased schedule and 128 transients per increment. The data points in the indirect dimensions were sampled nonuniformly with 25% of the total data points collected. 60° shifed sinebell squared apodization followed by Gaussian-to-Lorentzian transformations were utilized in the direct dimension, followed by zero-filling to 2048 points. Zero-filling to 128 points was used in the indirect dimensions. The final data point was collected at 10 ms. The total experiment time was 4 days. The first contour in all spectra is set at 5 times the noise level.

For a comprehensive discussion on NUS sampling methods see the recent review.[67] Although strides have been made toward optimizing NUS protocols, general understanding of the design principles is yet to be gained.

Application to Protein Assemblies: 1−73-(U-^{13}C,^{15}N)/74−108-(U-^{15}N) Reassembled Thioredoxin. To test the benefits of NUS in protein assemblies, we collected 2D NCA and NCACX, and 3D NCACX data for 1−73-(U-^{13}C,^{15}N)/74−108(U-^{15}N) thioredoxin reassembly. Reassembled thioredoxin is used by us as model system for developing and testing MAS NMR methodologies; with multiple benchmark 2D US data sets acquired by us,[53,54,56−58] it represents an ideal sample for the current study.

Figure 4 shows the comparison between the 2D NCA data: US/FFT (4A), NUS1/MINT (λ = 300) (4B), and NUS1/MINT (λ = 300) with additional 15 Hz line width deconvolution applied during data processing (4C). Remarkably, the 2D NUS/MINT spectrum (Figure 4B) contains nine new detectable peaks not present in the corresponding US/FFT data set recorded with the same experiment time (Figure 4A). The intensities of other cross-peaks are also generally higher in the NUS/MINT spectrum. Figure 4D displays 1D traces, showing consistently higher intensities in the NUS/MINT spectra.

The cross-peaks in the NUS1/MINT spectrum are broader in the indirect dimension compared with the US/FFT data, similar to our findings in MLF. To improve the resolution, a mild 15 Hz line width deconvolution was applied (Figure 4C), resulting in resolution similar to or better than the US/FFT spectrum. Although the sensitivity is somewhat reduced by line width deconvolution, most of the new peaks are still present in the spectrum. Interestingly, line width deconvolution works under MINT conditions, but not under conventional low-λ MaxEnt reconstruction (see Supporting Information Figure S4).

Not unexpectedly, a similar trend is observed for the 2D NCACX NUS data. Figure 5 displays the following spectra: US/FFT (A); NUS3/MINT (B); and NUS3/MINT, including 25 Hz line width deconvolution (C). Sixteen peaks that are either new or possess noticeably higher intensity were identified in the NUS data (see Figure 5). Remarkably, even with 25 Hz line width deconvolution 15 of the 16 peaks still appear (Figure 5C).

One of the most attractive features of NUS is the ability to attain required sensitivity and resolution while reducing

dx.doi.org/10.1021/jp3032786 | J. Phys. Chem. B 2012, 116, 7416−7427

otherwise long experiment times. This benefit is particularly important for higher-dimensionality experiments in which several indirect dimensions can be sampled nonuniformly. We collected a 3D NUS NCACX spectrum for 1−73-(U-^{13}C,^{15}N)/74−108-(U-^{15}N) reassembled thioredoxin. The corresponding US experiment is prohibitively long under our experimental conditions and could not be conducted. In Figure 5D, four 2D planes extracted from the 3D NUS/MaxEnt NCACX experiment are displayed; the data were processed with λ = 0.380 as optimized by RNMRTK, and without line width deconvolution. The spectrum exhibits excellent sensitivity and resolution. We have previously reported resonance assignments for this sample on the basis of the analysis of several 2D spectra.[56] We could not at the time collect any 3D data because of the sensitivity limitations.

The NUS protocol employed here permitted the acquisition of an high-quality 3D NCACX spectrum in 4 days, and the assignments, examples of which are presented in Figure 5D, are fully consistent with the previous 2D-based assignments. We note that for this size protein and given the excellent spectral resolution, only two 3D spectra (NCACX and NCOCX) are required for complete resonance assignments, using a fraction of instrument time required for acquisition of conventional US data sets and a fraction of data analysis time required for analysis of respective 2D spectra (backbone walks through 3D spectroscopy are much more straightforward than analysis of the multiple 2D data sets!). For this sample, using the 3D NUS schedule, only 25% of the total data points were retained, thus saving 75% of the experiment time while maintaining excellent sensitivity and resolution.

CONCLUSIONS AND FUTURE OUTLOOK

The use of nonuniform sampling for multidimensional solid-state NMR spectroscopy of biological systems is a promising venue. In solids, where often relatively short T_2^* times are observed, the benefit of sampling to evolution times of πT_2^*, where optimal resolution is attained, can be readily realized, as we have shown in this work. With an appropriate sampling schedule, gains in sensitivity of 1.5−1.7 fold can be achieved in each indirect dimension without compromising the spectral resolution. As demonstrated in thioredoxin reassembly, the NUS/MINT approach introduced here is highly advantageous for collecting high-quality multidimensional heteronuclear correlation spectra. NUS/MINT is anticipated to be particularly beneficial for three- and higher-dimensional data collection in biological systems that are either large or exhibit inherently low sensitivity or are unstable over time, rendering conventional multidimensional experiments impractical. The work presented in this manuscript was in large part motivated by having to overcome the sensitivity limitations while working with these kinds of challenging systems in our laboratory (e.g., microtubule-associated protein assemblies, HIV-1 protein assemblies, protein−inhibitor complexes), and we envision that NUS acquisition of multidimensional MAS NMR data sets will be highly advantageous for many other biological systems, as well.

ASSOCIATED CONTENT

Supporting Information

Figures with 3D NUS schedule used for the collection of 3D NCA and NCACX data sets on MLF and 1−73-(U-^{13}C,^{15}N)/74−108-(U-^{15}N) thioredoxin reassembly, stack plot of f_1 projections extracted from 3D NCACX spectra of MLF illustrating linearity of MaxEnt under MINT conditions. This material is available free of charge via the Internet at http://pubs.acs.org.

AUTHOR INFORMATION

Corresponding Author

*(D.R.) Phone: (570) 577-3676. E-mail: drovnyak@bucknell.edu. (T.P.) Phone: (302) 831-1968 E-mail: tpolenov@udel.edu.

Present Address

[§]Structural Biophysics Laboratory, Center for Cancer Research, National Cancer Institute, Frederick, MD.

Author Contributions

[∥]These authors contributed equally to this publication.

Notes

The authors declare no competing financial interest.

ACKNOWLEDGMENTS

This work was supported by the National Institutes of Health (NIH Grants R01GM085306, P50GM082251, P30GM103519 from NIGMS and P30RR031160 from NCRR to T.P.; P01GM47467 from NIGMS to J.C.H.; R15GM084443 from NIGMS to D.R.) and is a contribution from the Pittsburgh Center for HIV Protein Interactions. T.P. and C.S. thank Agilent, Inc. for partial support of this study. We thank Maria Luisa Tasayco and Dabeiba Marulanda for preparing the thioredoxin reassembly sample.

REFERENCES

(1) Hoch, J. C.; Maciejewski, M. W.; Mobli, M.; Schuyler, A. D.; Stern, A. S. *Nonuniform Sampling in Multidimensional NMR*; John Wiley: Chichester, 2012; In Press.

(2) Blumich, B. *J. Magn. Reson.* **1985**, *7*, 5−23.

(3) Mansfield, P. *Magn. Reson. Med.* **1984**, *1*, 370−386.

(4) Mishkovsky, M.; Frydman, L. *Annu. Rev. Phys. Chem.* **2009**, *60*, 429−448.

(5) Mobli, M.; Stern, A. S.; Hoch, J. C. *J. Magn. Reson.* **2006**, *182*, 96−105.

(6) Kim, S.; Szyperski, T. *J. Am. Chem. Soc.* **2003**, *125*, 1385−1393.

(7) Sibisi, S.; Skilling, J.; Brereton, R. G.; Laue, E. D.; Staunton, J. *Nature* **1984**, *311*, 446−447.

(8) Skilling, J.; R.K., B. *Mon. Not. R. Astr. Soc.* **1984**, *211*, 111−124.

(9) Hoch, J. C. *J. Magn. Reson.* **1985**, *64*, 436−440.

(10) Hore, P. J. *J. Magn. Reson.* **1985**, *62*, 561−567.

(11) Laue, E. D.; Skilling, J.; Staunton, J.; Sibisi, S.; Brereton, R. G. *J. Magn. Reson.* **1985**, *62*, 437−452.

(12) Davies, S. J.; Bauer, C.; Hore, P. J.; Freeman, R. *J. Magn. Reson.* **1988**, *76*, 476−493.

(13) Dereppe, J. M.; Jakus, N. *J. Magn. Reson.* **1988**, *79*, 307−317.

(14) Daniell, G. J.; Hore, P. J. *J. Magn. Reson.* **1989**, *84*, 515−536.

(15) Donoho, D. L.; Johnstone, I. M.; Stern, A. S.; Hoch, J. C. *Proc. Natl. Acad. Sci. U.S.A.* **1990**, *87*, 5066−5068.

(16) Hoch, J. C.; Stern, A. S.; Donoho, D. L.; Johnstone, I. M. *J. Magn. Reson.* **1990**, *86*, 236−246.

(17) Hoch, J. C.; Stern, A. S. *Maximum Entropy Reconstruction*; John Wiley & Sons: Chichester, 1996.

(18) Jeong, G. W.; Borer, P. N.; Wang, S. S.; Levy, G. C. *J. Magn. Reson.* **1993**, *103*, 123−134.

(19) Hyberts, S. G.; Frueh, D. P.; Arthanari, H.; Wagner, G. *J. Biomol. NMR* **2009**, *45*, 283−294.

(20) Hyberts, S. G.; Heffron, G. J.; Tarragona, N. G.; Solanky, K.; Edmonds, K. A.; Luithardt, H.; Fejzo, J.; Chorev, M.; Aktas, H.; Colson, K.; Falchuk, K. H.; Halperin, J. A.; Wagner, G. *J. Am. Chem. Soc.* **2007**, *129*, 5108−5116.

(21) Bruschweiler, R.; Zhang, F. L. *J. Chem. Phys.* **2004**, *120*, 5253−5260.

(22) Matsuki, Y.; Eddy, M. T.; Herzfeld, J. *J. Am. Chem. Soc.* **2009**, *131*, 4648−4656.
(23) Jaravine, V.; Ibraghimov, I.; Orekhov, V. Y. *Nat. Methods* **2006**, *3*, 605−607.
(24) Mandelshtam, V. A.; Taylor, H. S.; Shaka, A. J. *J. Magn. Reson.* **1998**, *133*, 304−312.
(25) Rovnyak, D.; Hoch, J. C.; Stern, A. S.; Wagner, G. *J. Biomol. NMR* **2004**, *30*, 1−10.
(26) Rovnyak, D.; Sarcone, M.; Jiang, Z. *Magn. Reson. Chem.* **2011**, *49*, 483−491.
(27) Astrof, N. S.; Lyon, C. E.; Griffin, R. G. *J. Magn. Reson.* **2001**, *152*, 303−3077.
(28) Franks, W. T.; Atreya, H. S.; Szyperski, T.; Rienstra, C. M. *J. Biomol. NMR* **2010**, *48*, 213−223.
(29) Heise, H.; Seidel, K.; Etzkorn, M.; Becker, S.; Baldus, M. *J. Magn. Reson.* **2005**, *173*, 64−74.
(30) Jones, D. H.; Opella, S. J. *J. Magn. Reson.* **2006**, *179*, 105−113.
(31) Matsuki, Y.; Eddy, M. T.; Griffin, R. G.; Herzfeld, J. *Angew. Chem., Int. Ed.* **2010**, *49*, 9215−9218.
(32) Qiang, W. *J. Magn. Reson.* **2011**, *213*, 171−175.
(33) Rovnyak, D.; Filip, C.; Itin, B.; Stern, A. S.; Wagner, G.; Griffin, R. G.; Hoch, J. C. *J. Magn. Reson.* **2003**, *161*, 43−55.
(34) Bayro, M. J.; Maly, T.; Birkett, N. R.; Macphee, C. E.; Dobson, C. M.; Griffin, R. G. *Biochemistry* **2010**, *49*, 7474−7484.
(35) Bertini, I.; Gonnelli, L.; Luchinat, C.; Mao, J.; Nesi, A. *J. Am. Chem. Soc.* **2011**, *133*, 16013−16022.
(36) Cady, S.; Wang, T.; Hong, M. *J. Am. Chem. Soc.* **2011**, *133*, 11572−11579.
(37) Fan, Y.; Shi, L.; Ladizhansky, V.; Brown, L. S. *J. Biomol. NMR* **2011**, *49*, 151−161.
(38) Habenstein, B.; Wasmer, C.; Bousset, L.; Sourigues, Y.; Schutz, A.; Loquet, A.; Meier, B. H.; Melki, R.; Bockmann, A. *J. Biomol. NMR* **2011**, *51*, 235−243.
(39) Han, Y.; Ahn, J.; Concel, J.; Byeon, I. J.; Gronenborn, A. M.; Yang, J.; Polenova, T. *J. Am. Chem. Soc.* **2010**, *132*, 1976−1987.
(40) Helmus, J. J.; Surewicz, K.; Apostol, M. I.; Surewicz, W. K.; Jaroniec, C. P. *J. Am. Chem. Soc.* **2011**, *133*, 13934−13937.
(41) Hou, G.; Byeon, I. J.; Ahn, J.; Gronenborn, A. M.; Polenova, T. *J. Am. Chem. Soc.* **2011**, *133*, 18646−18455.
(42) Hou, G.; Yan, S.; Sun, S.; Han, Y.; Byeon, I. J.; Ahn, J.; Concel, J.; Samoson, A.; Gronenborn, A. M.; Polenova, T. *J. Am. Chem. Soc.* **2011**, *133*, 3943−3953.
(43) Huang, L.; McDermott, A. E. *Biochim. Biophys. Acta* **2008**, *1777*, 1098−1108.
(44) Lewandowski, J. R.; van der Wel, P. C.; Rigney, M.; Grigorieff, N.; Griffin, R. G. *J. Am. Chem. Soc.* **2011**, *133*, 14686−14698.
(45) Renault, M.; Bos, M. P.; Tommassen, J.; Baldus, M. *J. Am. Chem. Soc.* **2011**, *133*, 4175−4177.
(46) Sun, S.; Butterworth, A. H.; Paramasivam, S.; Yan, S.; Lightcap, C. M.; Williams, J. C.; Polenova, T. *Can. J. Chem.* **2011**, *89*, 909−918.
(47) Sun, S.; Siglin, A.; Williams, J. C.; Polenova, T. *J. Am. Chem. Soc.* **2009**, *131*, 10113−10126.
(48) Tang, M.; Sperling, L. J.; Berthold, D. A.; Schwieters, C. D.; Nesbitt, A. E.; Nieuwkoop, A. J.; Gennis, R. B.; Rienstra, C. M. *J. Biomol. NMR* **2011**, *51*, 227−233.
(49) Tycko, R. *Annu. Rev. Phys. Chem.* **2011**, *62*, 279−299.
(50) Tycko, R.; Savtchenko, R.; Ostapchenko, V. G.; Makarava, N.; Baskakov, I. V. *Biochemistry* **2010**, *49*, 9488−9497.
(51) Xu, J.; Soong, R.; Im, S. C.; Waskell, L.; Ramamoorthy, A. *J. Am. Chem. Soc.* **2010**, *132*, 9944−9947.
(52) Yi, M.; Cross, T. A.; Zhou, H. X. *Proc. Natl. Acad. Sci. U.S.A.* **2009**, *106*, 13311−13316.
(53) Marulanda, D.; Tasayco, M. L.; Cataldi, M.; Arriaran, V.; Polenova, T. *J. Phys. Chem. B* **2005**, *109*, 18135−18145.
(54) Marulanda, D.; Tasayco, M. L.; McDermott, A.; Cataldi, M.; Arriaran, V.; Polenova, T. *J. Am. Chem. Soc.* **2004**, *126*, 16608−16620.
(55) Sun, S.; Han, Y.; Paramasivam, S.; Yan, S.; Siglin, A. E.; Williams, J. C.; Byeon, I. J.; Ahn, J.; Gronenborn, A. M.; Polenova, T. *Methods Mol. Biol.* **2012**, *831*, 303−331.
(56) Yang, J.; Paramasivam, S.; Marulanda, D.; Cataldi, M.; Tasayco, M. L.; Polenova, T. *Magn. Reson. Chem.* **2007**, *45*, S73−S83.
(57) Yang, J.; Tasayco, M. L.; Polenova, T. *J. Am. Chem. Soc.* **2008**, *130*, 5798−5807.
(58) Yang, J.; Tasayco, M. L.; Polenova, T. *J. Am. Chem. Soc.* **2009**, *131*, 13690−13702.
(59) Yu, W. F.; Tung, C. S.; Wang, H.; Tasayco, M. L. *Protein Sci.* **2000**, *9*, 20−28.
(60) States, D. J.; Haberkorn, R. A.; Ruben, D. J. *J. Magn. Reson.* **1982**, *48*, 286−292.
(61) Hoch, J. C.; Stern, A. S. *NMR Data Processing*; Wiley-Liss: NewYork, 1996.
(62) Goddard, T. D.; Kneller, D. G. *SPARKY3*; University of California, San Francisco.
(63) Eddy, M. T.; Ruben, D.; Griffin, R. G.; Herzfeld, J. *J. Magn. Reson.* **2012**, *214*, 296−301.
(64) Ni, F.; Scheraga, H. A. *J. Magn. Reson.* **1986**, *70*, 506−511.
(65) Stern, A. S.; Li, K. B.; Hoch, J. C. *J. Am. Chem. Soc.* **2002**, *124*, 1982−1993.
(66) Hyberts, S. G.; Takeuchi, K.; Wagner, G. *J. Am. Chem. Soc.* **2010**, *132*, 2145−2147.
(67) Maciejewski, M. W.; Mobli, M.; Schuyler, A. D.; Stern, A. S.; Hoch, J. C. *Top. Curr. Chem.* **2012**, *316*, 49−77.